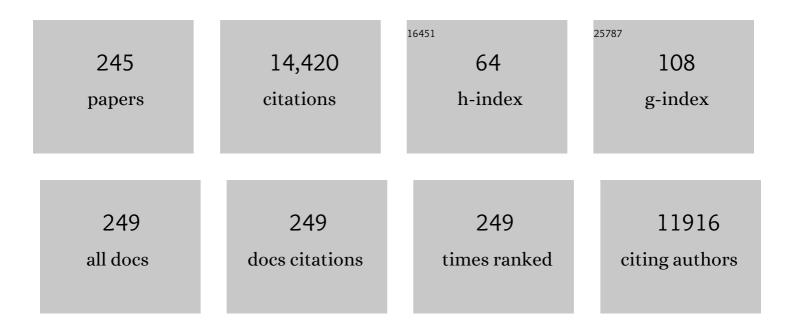
## Hongping He

List of Publications by Year in descending order

Source: https://exaly.com/author-pdf/5773432/publications.pdf Version: 2024-02-01



HONCRING HE

#	Article	IF	CITATIONS
1	Incorporation of incompatible trace elements into molybdenite: Layered PbS precipitates within molybdenite. American Mineralogist, 2022, 107, 54-64.	1.9	8
2	Magnetite-rutile symplectite in ilmenite records magma hydration in layered intrusions. American Mineralogist, 2022, 107, 395-404.	1.9	4
3	Periodic and non-periodic stacking in molybdenite (MoS2) revealed by STEM. American Mineralogist, 2022, 107, 997-1006.	1.9	6
4	FEASIBILITY OF VISIBLE SHORT-WAVE INFRARED REFLECTANCE SPECTROSCOPY TO CHARACTERIZE REGOLITH-HOSTED RARE EARTH ELEMENT MINERALIZATION. Economic Geology, 2022, 117, 495-508.	3.8	3
5	Distinct effects of transition metal (cobalt, manganese and nickel) ion substitutions on the abiotic oxidation of pyrite: In view of hydroxyl radical production. Geochimica Et Cosmochimica Acta, 2022, 321, 170-183.	3.9	6
6	Environmental risk assessment of the potential "Chemical Time Bomb―of ion-adsorption type rare earth elements in urban areas. Science of the Total Environment, 2022, 822, 153305.	8.0	24
7	The Composition and Growth Mechanism of Coexisting 4M2 and 4A8 Biotite Polytypes from Rhyolite of Long Valley Caldera, California. Clays and Clay Minerals, 2022, 70, 48-61.	1.3	1
8	Competitive adsorption of alkali ions on aqueous mica surface: A force field comparison molecular dynamics study. Applied Clay Science, 2022, 219, 106436.	5.2	7
9	Transformation of Ordered Albite into Kaolinite: Implication for the "Booklet―Morphology. ACS Earth and Space Chemistry, 2022, 6, 1133-1142.	2.7	3
10	Superimposed microstructures of pyrite in auriferous quartz veins as fingerprints of episodic fluid infiltration in the Wulong Lode gold deposit, NE China. Mineralium Deposita, 2022, 57, 685-700.	4.1	7
11	Photoreductive Dissolution of Iron (Hydr)oxides and Its Geochemical Significance. ACS Earth and Space Chemistry, 2022, 6, 811-829.	2.7	14
12	Reduction of acid mine drainage by passivation of pyrite surfaces: A review. Science of the Total Environment, 2022, 832, 155116.	8.0	26
13	The different effects of sulfate on the adsorption of REEs on kaolinite and ferrihydrite. Applied Clay Science, 2022, 221, 106468.	5.2	6
14	Carbonate accelerated transformation of ferrihydrite in the presence of phosphate. Geoderma, 2022, 417, 115811.	5.1	4
15	Enhanced immobilization of phosphate by ferrihydrite during the photoreductive dissolution process. Science of the Total Environment, 2022, 838, 155835.	8.0	1
16	Weathering of Chlorite Illite Deposits in the Hyperarid Qaidam Basin: Implications to Post-Depositional Alteration on Martian Clay Minerals. Frontiers in Astronomy and Space Sciences, 2022, 9, .	2.8	1
17	Microorganisms Accelerate REE Mineralization in Supergene Environments. Applied and Environmental Microbiology, 2022, 88, .	3.1	9
18	Multiple Growth Mechanisms of 2:1 Type Layered Aluminosilicates during Mineral Transformation. ACS Earth and Space Chemistry, 2022, 6, 1930-1936.	2.7	0

#	Article	IF	CITATIONS
19	Coupled redox cycling of Fe and Mn in the environment: The complex interplay of solution species with Fe- and Mn-(oxyhydr)oxide crystallization and transformation. Earth-Science Reviews, 2022, 232, 104105.	9.1	25
20	Competitive adsorption geometries for the arsenate As(V) and phosphate P(V) oxyanions on magnetite surfaces: Experiments and theory. American Mineralogist, 2021, 106, 374-388.	1.9	24
21	Massive Deposition of Carbonate Nodules in the Hyperarid Northwest Qaidam Basin of the Northern Tibetan Plateau. Geochemistry, Geophysics, Geosystems, 2021, 22, e2021GC009654.	2.5	3
22	Environmental-sulfur-controlled surface properties of pyrite: a first principles PBE + U study. Physics and Chemistry of Minerals, 2021, 48, 1.	0.8	6
23	Fluid pathway evolution and mass transfer during Mg-dominated mineral transformations. Applied Clay Science, 2021, 207, 106097.	5.2	0
24	Development of novel multifunctional adsorbent by effectively hosting both zwitterionic surfactant and hydrated ferric oxides in montmorillonite. Science of the Total Environment, 2021, 774, 144974.	8.0	6
25	Evidence for a two-stage particle attachment mechanism for phyllosilicate crystallization in geological processes. American Mineralogist, 2021, 106, 983-993.	1.9	6
26	Technical development of characterization methods provides insights into clay mineral-water interactions: A comprehensive review. Applied Clay Science, 2021, 206, 106088.	5.2	26
27	REE fractionation controlled by REE speciation during formation of the Renju regolith-hosted REE deposits in Guangdong Province, South China. Ore Geology Reviews, 2021, 134, 104172.	2.7	20
28	Brain-terrain-like features in the Qaidam Basin: Implications for various morphological features on Mars. Icarus, 2021, 363, 114434.	2.5	2
29	Characteristics and genesis of ion adsorption type REE deposits in the weathering crusts of metamorphic rocks in Ningdu, Ganzhou, China. Ore Geology Reviews, 2021, 135, 104173.	2.7	21
30	Uranium re-adsorption on uranium mill tailings and environmental implications. Journal of Hazardous Materials, 2021, 416, 126153.	12.4	51
31	Facet-specific oxidation of Mn(II) and heterogeneous growth of manganese (oxyhydr)oxides on hematite nanoparticles. Geochimica Et Cosmochimica Acta, 2021, 307, 151-167.	3.9	21
32	Groundwater controls REE mineralisation in the regolith of South China. Chemical Geology, 2021, 577, 120295.	3.3	18
33	Ferrihydrite Transformation Impacted by Adsorption and Structural Incorporation of Rare Earth Elements. ACS Earth and Space Chemistry, 2021, 5, 2768-2777.	2.7	9
34	An abiotic source of Archean hydrogen peroxide and oxygen that pre-dates oxygenic photosynthesis. Nature Communications, 2021, 12, 6611.	12.8	41
35	Visible/near infrared reflectance (VNIR) spectral features of ion-exchangeable Rare earth elements hosted by clay minerals: Potential use for exploration of regolith-hosted REE deposits. Applied Clay Science, 2021, 215, 106320.	5.2	3
36	Functionalized layered double hydroxides for innovative applications. Materials Horizons, 2020, 7, 715-745.	12.2	171

#	Article	IF	CITATIONS
37	Closest-Packing Water Monolayer Stably Intercalated in Phyllosilicate Minerals under High Pressure. Langmuir, 2020, 36, 618-627.	3.5	7
38	A novel multifunctional adsorbent synthesized by modifying acidified organo-montmorillonite with iron hydroxides. Applied Clay Science, 2020, 185, 105420.	5.2	24
39	Layered intercalation compounds: Mechanisms, new methodologies, and advanced applications. Progress in Materials Science, 2020, 109, 100631.	32.8	66
40	Carbonate-Enhanced Transformation of Ferrihydrite to Hematite. Environmental Science & Technology, 2020, 54, 13701-13708.	10.0	25
41	Organoclay-derived lamellar silicon carbide/carbon composite as an ideal support for Pt nanoparticles: facile synthesis and toluene oxidation performance. Chemical Communications, 2020, 56, 9489-9492.	4.1	3
42	Coupling between clay swelling/collapse and cationic partition. Geochimica Et Cosmochimica Acta, 2020, 285, 78-99.	3.9	29
43	Formation of Misfit Layered PbS Within Molybdenite. Microscopy and Microanalysis, 2020, 26, 486-487.	0.4	0
44	Diatomite-Metal-Organic Framework Composite with Hierarchical Pore Structures for Adsorption/Desorption of Hydrogen, Carbon Dioxide and Water Vapor. Materials, 2020, 13, 4700.	2.9	13
45	Intrinsic water layering next to soft, solid, hydrophobic, and hydrophilic substrates. Journal of Chemical Physics, 2020, 153, 224702.	3.0	1
46	Kaolinization of 2:1 type clay minerals with different swelling properties. American Mineralogist, 2020, 105, 687-696.	1.9	23
47	Effects of Fullerol and Graphene Oxide on the Phase Transformation of Two-Line Ferrihydrite. ACS Earth and Space Chemistry, 2020, 4, 335-344.	2.7	16
48	One-pot synthesis of the reduced-charge montmorillonite via molten salts treatment. Applied Clay Science, 2020, 186, 105429.	5.2	6
49	Heterogeneous Nucleation and Growth of CaCO3 on Calcite (104) and Aragonite (110) Surfaces: Implications for the Formation of Abiogenic Carbonate Cements in the Ocean. Minerals (Basel,) Tj ETQq1 1 0.784	4324orgBT	- /Overlock 1
50	CNTs/ferrihydrite as a highly efficient heterogeneous Fenton catalyst for the degradation of bisphenol A: The important role of CNTs in accelerating Fe(III)/Fe(II) cycling. Applied Catalysis B: Environmental, 2020, 270, 118891.	20.2	152
51	Pressure-temperature diagram of wetting and dewetting in a hydrophobic grain boundary and the liquidlike to icelike transition of monolayer water. Physical Review B, 2020, 101, .	3.2	3
52	Formation of saponite by hydrothermal alteration of metal oxides: Implication for the rarity of hydrotalcite. American Mineralogist, 2019, 104, 1156-1164.	1.9	6
53	Adsorption of REEs on kaolinite and halloysite: A link to the REE distribution on clays in the weathering crust of granite. Chemical Geology, 2019, 525, 210-217.	3.3	100
54	Keggin-Al30: An intercalant for Keggin-Al30 pillared montmorillonite. Applied Clay Science, 2019, 180, 105203.	5.2	16

#	Article	IF	CITATIONS
55	Transformation of boehmite into 2:1 type layered aluminosilicates with different layer charges under hydrothermal conditions. Applied Clay Science, 2019, 181, 105207.	5.2	7
56	The structural change of vermiculite during dehydration processes: A real-time in-situ XRD method. Applied Clay Science, 2019, 183, 105332.	5.2	26
57	Preservation of Cyanobacterial UVRâ€Shielding Pigment Scytonemin in Carbonate Ooids Formed in Pleistocene Salt Lakes in the Qaidam Basin, Tibetan Plateau. Geophysical Research Letters, 2019, 46, 10375-10383.	4.0	11
58	Crystal habit-directed gold deposition on pyrite: Surface chemical interpretation of the pyrite morphology indicative of gold enrichment. Geochimica Et Cosmochimica Acta, 2019, 264, 191-204.	3.9	24
59	Sequestration of Gaseous Hg <sup>0</sup> by Sphalerite with Fe Substitution: Performance, Mechanism, and Structure–Activity Relationship. Journal of Physical Chemistry C, 2019, 123, 2828-2836.	3.1	21
60	<i>In situ</i> synthesis of a silicon flake/nitrogen-doped graphene-like carbon composite from organoclay for high-performance lithium-ion battery anodes. Chemical Communications, 2019, 55, 2644-2647.	4.1	44
61	The distinct effects of substitution and deposition of Ag in perovskite LaCoO3 on the thermally catalytic oxidation of toluene. Applied Surface Science, 2019, 489, 905-912.	6.1	47
62	Strategies for enhancing the heterogeneous Fenton catalytic reactivity: A review. Applied Catalysis B: Environmental, 2019, 255, 117739.	20.2	687
63	Kinetics and mechanisms of the interaction between the calcite (10.4) surface and Cu2+-bearing solutions. Science of the Total Environment, 2019, 668, 602-616.	8.0	17
64	Heterogeneous Reduction of 2-Chloronitrobenzene by Co-substituted Magnetite Coupled with Aqueous Fe <sup>2+</sup> : Performance, Factors, and Mechanism. ACS Earth and Space Chemistry, 2019, 3, 728-737.	2.7	7
65	Understanding the role of natural clay minerals as effective adsorbents and alternative source of rare earth elements: Adsorption operative parameters. Hydrometallurgy, 2019, 185, 149-161.	4.3	76
66	The catalytic oxidation of formaldehyde over palygorskite-supported copper and manganese oxides: Catalytic deactivation and regeneration. Applied Surface Science, 2019, 464, 287-293.	6.1	64
67	Chemical and structural studies of coexisting 1M- and 2M1-polytypes in synthetic fluorophlogopites and influence of Al on the polytype formation. Physics and Chemistry of Minerals, 2019, 46, 259-270.	0.8	3
68	Arrangement Models of Keggin-Al <sub>30</sub> and Keggin-Al <sub>13</sub> in the Interlayer of Montmorillonite and the Impacts of Pillaring on Surface Acidity: A Comparative Study on Catalytic Oxidation of Toluene. Langmuir, 2019, 35, 382-390.	3.5	25
69	TiO2/Schwertmannite nanocomposites as superior co-catalysts in heterogeneous photo-Fenton process. Journal of Environmental Sciences, 2019, 80, 208-217.	6.1	17
70	The mechanism of defect induced hydroxylation on pyrite surfaces and implications for hydroxyl radical generation in prebiotic chemistry. Geochimica Et Cosmochimica Acta, 2019, 244, 163-172.	3.9	26
71	Degradation of 2,4-dichlorophenol using palygorskite-supported bimetallic Fe/Ni nanocomposite as a heterogeneous catalyst. Applied Clay Science, 2019, 168, 276-286.	5.2	40
72	Remarkable effect of Co substitution in magnetite on the reduction removal of Cr(VI) coupled with aqueous Fe(II): Improvement mechanism and Cr fate. Science of the Total Environment, 2019, 656, 400-408.	8.0	14

#	Article	IF	CITATIONS
73	Self-templating synthesis of silicon nanorods from natural sepiolite for high-performance lithium-ion battery anodes. Journal of Materials Chemistry A, 2018, 6, 6356-6362.	10.3	67
74	Enhanced photoelectrochemical degradation of Ibuprofen and generation of hydrogen via BiOI-deposited TiO2 nanotube arrays. Science of the Total Environment, 2018, 633, 1198-1205.	8.0	27
75	Heterogeneous photo-Fenton degradation of bisphenol A over Ag/AgCl/ferrihydrite catalysts under visible light. Chemical Engineering Journal, 2018, 346, 567-577.	12.7	157
76	Catalytic degradation of Orange II in aqueous solution using diatomite-supported bimetallic Fe/Ni nanoparticles. RSC Advances, 2018, 8, 7687-7696.	3.6	29
77	Superior thermal stability of Keggin-Al 30 pillared montmorillonite: A comparative study with Keggin-Al 13 pillared montmorillonite. Microporous and Mesoporous Materials, 2018, 265, 104-111.	4.4	25
78	Improvement of zinc substitution in the reactivity of magnetite coupled with aqueous Fe(II) towards nitrobenzene reduction. Journal of Colloid and Interface Science, 2018, 517, 104-112.	9.4	12
79	Pyrolysis behaviors of organic matter (OM) with the same alkyl main chain but different functional groups in the presence of clay minerals. Applied Clay Science, 2018, 153, 205-216.	5.2	27
80	Surface structure-dependent pyrite oxidation in relatively dry and moist air: Implications for the reaction mechanism and sulfur evolution. Geochimica Et Cosmochimica Acta, 2018, 228, 259-274.	3.9	58
81	Selective loading of 5-fluorouracil in the interlayer space of methoxy-modified kaolinite for controlled release. Applied Clay Science, 2018, 159, 102-106.	5.2	58
82	Interaction of polyhydroxy fullerenes with ferrihydrite: adsorption and aggregation. Journal of Environmental Sciences, 2018, 64, 1-9.	6.1	18
83	Effect of acid activation of palygorskite on their toluene adsorption behaviors. Applied Clay Science, 2018, 159, 60-67.	5.2	83
84	Structural effects on dissolution of silica polymorphs in various solutions. Inorganica Chimica Acta, 2018, 471, 57-65.	2.4	9
85	Synergistic adsorption of Cd(II) with sulfate/phosphate on ferrihydrite: An in situ ATR-FTIR/2D-COS study. Chemical Geology, 2018, 477, 12-21.	3.3	75
86	Adsorption of ammonium by different natural clay minerals: Characterization, kinetics and adsorption isotherms. Applied Clay Science, 2018, 159, 83-93.	5.2	218
87	Mineralogical Evolution of the Paleogene Formations in the Kyzyltokoy Basin, Kyrgyzstan: Implications for the Formation of Glauconite. Clays and Clay Minerals, 2018, 66, 43-60.	1.3	3
88	Conversion of serpentine to smectite under hydrothermal condition: Implication for solid-state transformation. American Mineralogist, 2018, 103, 241-251.	1.9	25
89	Hydration induced bandgap shift at pyrite-water interface. Applied Physics Letters, 2018, 113, .	3.3	3
90	Clay minerals derived nanostructured silicon with various morphology: Controlled synthesis, structural evolution, and enhanced lithium storage properties. Journal of Power Sources, 2018, 405, 61-69.	7.8	34

#	Article	IF	CITATIONS
91	Synergetic effect of Cu and Mn oxides supported on palygorskite for the catalytic oxidation of formaldehyde: Dispersion, microstructure, and catalytic performance. Applied Clay Science, 2018, 161, 265-273.	5.2	55
92	Superior adsorption of phosphate by ferrihydrite-coated and lanthanum-decorated magnetite. Journal of Colloid and Interface Science, 2018, 530, 704-713.	9.4	185
93	Visible-light Ag/AgBr/ferrihydrite catalyst with enhanced heterogeneous photo-Fenton reactivity via electron transfer from Ag/AgBr to ferrihydrite. Applied Catalysis B: Environmental, 2018, 239, 280-289.	20.2	123
94	Influences of Cation Ratio, Anion Type, and Water Content on Polytypism of Layered Double Hydroxides. Inorganic Chemistry, 2018, 57, 7299-7313.	4.0	27
95	Keggin-Al 30 pillared montmorillonite. Microporous and Mesoporous Materials, 2017, 242, 256-263.	4.4	39
96	Novel intercalation mechanism of zwitterionic surfactant modified montmorillonites. Applied Clay Science, 2017, 141, 265-271.	5.2	50
97	Mechanisms for the enhanced photo-Fenton activity of ferrihydrite modified with BiVO 4 at neutral pH. Applied Catalysis B: Environmental, 2017, 212, 50-58.	20.2	182
98	Nanogeosciences: Research History, Current Status, and Development Trends. Journal of Nanoscience and Nanotechnology, 2017, 17, 5930-5965.	0.9	67
99	Reduction removal of hexavalent chromium by zinc-substituted magnetite coupled with aqueous Fe(II) at neutral pH value. Journal of Colloid and Interface Science, 2017, 500, 20-29.	9.4	23
100	Influence of interlayer species on the thermal characteristics of montmorillonite. Applied Clay Science, 2017, 135, 129-135.	5.2	41
101	Temperature-Dependent Structure and Dynamics of Water Intercalated in Layered Double Hydroxides with Different Hydration States. Journal of Physical Chemistry C, 2017, 121, 23752-23762.	3.1	10
102	H <sub>2</sub> S-Modified Natural Ilmenite: A Recyclable Magnetic Sorbent for Recovering Gaseous Elemental Mercury from Flue Gas. Industrial & Engineering Chemistry Research, 2017, 56, 10060-10068.	3.7	29
103	Preparation of functionalized kaolinite/epoxy resin nanocomposites with enhanced thermal properties. Applied Clay Science, 2017, 148, 103-108.	5.2	43
104	Adsorption isotherm, mechanism, and geometry of Pb(II) on magnetites substituted with transition metals. Chemical Geology, 2017, 470, 132-140.	3.3	37
105	Microwave-Assisted Synthesis of Fe <sub>3</sub> O <sub>4</sub> Nanocrystals with Predominantly Exposed Facets and Their Heterogeneous UVA/Fenton Catalytic Activity. ACS Applied Materials & Interfaces, 2017, 9, 29203-29212.	8.0	91
106	Converting Spent Cu/Fe Layered Double Hydroxide into Cr(VI) Reductant and Porous Carbon Material. Scientific Reports, 2017, 7, 7277.	3.3	28
107	Photochemically Induced Electron Transfer: Simultaneously Decolorizing Dye and Reducing Cr(VI). Water, Air, and Soil Pollution, 2017, 228, 1.	2.4	4
108	Transformation of halloysite and kaolinite into beidellite under hydrothermal condition. American Mineralogist, 2017, 102, 997-1005.	1.9	20

#	Article	IF	CITATIONS
109	Molecular Simulation Study on the Interaction of Nanoparticles with Clay Minerals: C <sub>60</sub> on Surfaces of Pyrophyllite and Kaolinite. Clays and Clay Minerals, 2017, 65, 398-409.	1.3	4
110	Magnetite exsolution in ilmenite from the Fe-Ti oxide gabbro in the Xinjie intrusion (SW China) and sources of unusually strong remnant magnetization. American Mineralogist, 2016, 101, 2759-2767.	1.9	15
111	Morphology controllable syntheses of micro- and nano-iron pyrite mono- and poly-crystals: a review. RSC Advances, 2016, 6, 31988-31999.	3.6	22
112	Bisphenol A degradation by a new acidic nano zero-valent iron diatomite composite. Catalysis Science and Technology, 2016, 6, 6066-6075.	4.1	34
113	Fullerene modification of Ag <sub>3</sub> PO <sub>4</sub> for the visible-light-driven degradation of acid red 18. RSC Advances, 2016, 6, 85962-85969.	3.6	15
114	Aggregative growth of quasi-octahedral iron pyrite mesocrystals in a polyol solution through oriented attachment. CrystEngComm, 2016, 18, 8823-8828.	2.6	12
115	Fullerol modification ferrihydrite for the degradation of acid red 18 under simulated sunlight irradiation. Journal of Molecular Catalysis A, 2016, 424, 393-401.	4.8	24
116	Performance of Ti-pillared montmorillonite supported Fe catalysts for toluene oxidation: The effect of Fe on catalytic activity. Applied Clay Science, 2016, 132-133, 96-104.	5.2	47
117	Silylation of saponite with 3-aminopropyltriethoxysilane. Applied Clay Science, 2016, 132-133, 133-139.	5.2	37
118	BiVO4/Fe/Mt composite for visible-light-driven degradation of acid red 18. Applied Clay Science, 2016, 129, 27-34.	5.2	21
119	Visible light assisted Fenton-like degradation of Orange II on Ni 3 Fe/Fe 3 O 4 magnetic catalyst prepared from spent FeNi layered double hydroxide. Journal of Molecular Catalysis A, 2016, 415, 9-16.	4.8	41
120	Adsorbents based on montmorillonite for contaminant removal from water: A review. Applied Clay Science, 2016, 123, 239-258.	5.2	389
121	Preparation of surface-functionalized porous clay heterostructures via carbonization of soft-template and their adsorption performance for toluene. Applied Surface Science, 2016, 363, 113-121.	6.1	43
122	Ag <sub>3</sub> PO <sub>4</sub> immobilized on hydroxy-metal pillared montmorillonite for the visible light driven degradation of acid red 18. Catalysis Science and Technology, 2016, 6, 4116-4123.	4.1	35
123	Efficiency of Fe–montmorillonite on the removal of Rhodamine B and hexavalent chromium from aqueous solution. Applied Clay Science, 2016, 120, 9-15.	5.2	53
124	The variation of cationic microstructure in Mn-doped spinel ferrite during calcination and its effect on formaldehyde catalytic oxidation. Journal of Hazardous Materials, 2016, 306, 305-312.	12.4	38
125	Adsorption of phenol, phosphate and Cd(II) by inorganic–organic montmorillonites: A comparative study of single and multiple solute. Colloids and Surfaces A: Physicochemical and Engineering Aspects, 2016, 497, 63-71.	4.7	43
126	A new insight into the compositional and structural control of porous clay heterostructures from the perspective of NMR and TEM. Microporous and Mesoporous Materials, 2016, 224, 285-293.	4.4	20

#	Article	IF	CITATIONS
127	Facile synthesis of nitrogen and sulfur co-doped graphene-like carbon materials using methyl blue/montmorillonite composites. Microporous and Mesoporous Materials, 2016, 225, 137-143.	4.4	33
128	Co-adsorption of phosphate and zinc(II) on the surface of ferrihydrite. Chemosphere, 2016, 144, 1148-1155.	8.2	118
129	Adsorption of phenol and Cu(II) onto cationic and zwitterionic surfactant modified montmorillonite in single and binary systems. Chemical Engineering Journal, 2016, 283, 880-888.	12.7	112
130	Effect of Mn substitution on the promoted formaldehyde oxidation over spinel ferrite: Catalyst characterization, performance and reaction mechanism. Applied Catalysis B: Environmental, 2016, 182, 476-484.	20.2	149
131	Possible mechanism of structural incorporation of Al into diatomite during the deposition process I. Via a condensation reaction of hydroxyl groups. Journal of Colloid and Interface Science, 2016, 461, 64-68.	9.4	10
132	Methoxy-modified kaolinite as a novel carrier for high-capacity loading and controlled-release of the herbicide amitrole. Scientific Reports, 2015, 5, 8870.	3.3	46
133	Surface silylation of natural mesoporous/macroporous diatomite for adsorption of benzene. Journal of Colloid and Interface Science, 2015, 448, 545-552.	9.4	52
134	Thermal analysis evidence for the location of zwitterionic surfactant on clay minerals. Applied Clay Science, 2015, 112-113, 62-67.	5.2	27
135	Organo-Clays As Sorbents of Hydrophobic Organic Contaminants: Sorptive Characteristics and Approaches to Enhancing Sorption Capacity. Clays and Clay Minerals, 2015, 63, 199-221.	1.3	32
136	Simultaneous adsorption of Cd( <scp>ii</scp> ) and phosphate on Al <sub>13</sub> pillared montmorillonite. RSC Advances, 2015, 5, 77227-77234.	3.6	39
137	The structure of montmorillonites modified with zwitterionic surfactants and their sorption ability. Mineralogy and Petrology, 2015, 109, 349-355.	1.1	10
138	Modelling the effects of surfactant loading level on the sorption of organic contaminants on organoclays. RSC Advances, 2015, 5, 47022-47030.	3.6	24
139	From spent Mg/Al layered double hydroxide to porous carbon materials. Journal of Hazardous Materials, 2015, 300, 572-580.	12.4	28
140	The oxidation state and microstructural environment of transition metals (V, Co, and Ni) in magnetite: an XAFS study. Physics and Chemistry of Minerals, 2015, 42, 373-383.	0.8	16
141	Natural Magnetite: an efficient catalyst for the degradation of organic contaminant. Scientific Reports, 2015, 5, 10139.	3.3	55
142	Magnetite-rutile symplectite derived from ilmenite-hematite solid solution in the Xinjie Fe-Ti oxide-bearing, mafic-ultramafic layered intrusion (SW China). American Mineralogist, 2015, 100, 2348-2351.	1.9	22
143	The non-micellar template model for porous clay heterostructures: A perspective from the layer charge of base clay. Applied Clay Science, 2015, 116-117, 102-110.	5.2	19
144	Templated synthesis of nitrogen-doped graphene-like carbon materials using spent montmorillonite. RSC Advances, 2015, 5, 7522-7528.	3.6	34

#	Article	IF	CITATIONS
145	Heterogeneous activation of Oxone by substituted magnetites Fe3â^'xMxO4 (Cr, Mn, Co, Ni) for degradation of Acid Orange II at neutral pH. Journal of Molecular Catalysis A, 2015, 398, 86-94.	4.8	114
146	Effects of organic templates on the structural properties of porous clay heterostructures: a non-micellar template model for porous structure. Journal of Porous Materials, 2015, 22, 219-228.	2.6	9
147	Aluminum ion occupancy in the structure of synthetic saponites: Effect on crystallinity. American Mineralogist, 2014, 99, 109-116.	1.9	26
148	Investigation of structure and thermal stability of surfactant-modified Al-pillared montmorillonite. Journal of Thermal Analysis and Calorimetry, 2014, 115, 219-225.	3.6	13
149	Tailoring surface properties and structure of layered double hydroxides using silanes with different number of functional groups. Journal of Solid State Chemistry, 2014, 213, 176-181.	2.9	30
150	Synthesis of organoclays: A critical review and some unresolved issues. Applied Clay Science, 2014, 100, 22-28.	5.2	136
151	High-capacity loading of 5-fluorouracil on the methoxy-modified kaolinite. Applied Clay Science, 2014, 100, 60-65.	5.2	39
152	The distinct effects of Mn substitution on the reactivity of magnetite in heterogeneous Fenton reaction and Pb(II) adsorption. Journal of Colloid and Interface Science, 2014, 426, 181-189.	9.4	40
153	Restricting layer collapse enhances the adsorption capacity of reduced-charge organoclays. Applied Clay Science, 2014, 88-89, 73-77.	5.2	17
154	Surface Heterogeneity of SiO <sub>2</sub> Polymorphs: An XPS Investigation of α-Quartz and α-Cristobalite. Journal of Physical Chemistry C, 2014, 118, 26249-26257.	3.1	41
155	Al13-pillared montmorillonite modified by cationic and zwitterionic surfactants: A comparative study. Applied Clay Science, 2014, 101, 327-334.	5.2	13
156	Structure and dynamic properties of water saturated CTMA-montmorillonite: molecular dynamics simulations. Applied Clay Science, 2014, 97-98, 62-71.	5.2	30
157	Silylation of Al13-intercalated montmorillonite with trimethylchlorosilane and their adsorption for Orange II. Applied Clay Science, 2014, 99, 229-236.	5.2	28
158	Co-sorption of Cd and phosphate on the surface of a synthetic hydroxyiron-montmorillonite complex. Clays and Clay Minerals, 2014, 62, 79-88.	1.3	26
159	From used montmorillonite to carbon monolayer–montmorillonite nanocomposites. Applied Clay Science, 2014, 100, 112-117.	5.2	39
160	Montmorillonite as a multifunctional adsorbent can simultaneously remove crystal violet, cetyltrimethylammonium, and 2-naphthol from water. Applied Clay Science, 2014, 88-89, 33-38.	5.2	43
161	Effect of functionalized kaolinite on the curing kinetics of cycloaliphatic epoxy/anhydride system. Applied Clay Science, 2014, 95, 317-322.	5.2	19
162	The constraints of transition metal substitutions (Ti, Cr, Mn, Co and Ni) in magnetite on its catalytic activity in heterogeneous Fenton and UV/Fenton reaction: From the perspective of hydroxyl radical generation. Applied Catalysis B: Environmental, 2014, 150-151, 612-618.	20.2	130

#	Article	IF	CITATIONS
163	Effects of solid acidity of clay minerals on the thermal decomposition of 12-aminolauric acid. Journal of Thermal Analysis and Calorimetry, 2013, 114, 125-130.	3.6	15
164	The valence and site occupancy of substituting metals in magnetite spinel structure Fe3â^'xMxO4 (MÂ=ÂCr, Mn, Co and Ni) and their influence on thermal stability: An XANES and TG-DSC investigation. Solid State Sciences, 2013, 15, 115-122.	3.2	75
165	Studies on the solid acidity of heated and cation-exchanged montmorillonite using n-butylamine titration in non-aqueous system and diffuse reflectance Fourier transform infrared (DRIFT) spectroscopy. Physics and Chemistry of Minerals, 2013, 40, 479-489.	0.8	13
166	Quantitative characterization of the solid acidity of montmorillonite using combined FTIR and TPD based on the NH3 adsorption system. Applied Clay Science, 2013, 80-81, 407-412.	5.2	134
167	The influence of substituting metals (Ti, V, Cr, Mn, Co and Ni) on the thermal stability of magnetite. Journal of Thermal Analysis and Calorimetry, 2013, 111, 1317-1324.	3.6	19
168	Silylation of montmorillonite surfaces: Dependence on solvent nature. Journal of Colloid and Interface Science, 2013, 391, 16-20.	9.4	59
169	Silylation of clay mineral surfaces. Applied Clay Science, 2013, 71, 15-20.	5.2	134
170	Thermal degradation of organic matter in the interlayer clay–organic complex: A TG-FTIR study on a montmorillonite/12-aminolauric acid system. Applied Clay Science, 2013, 80-81, 398-406.	5.2	48
171	The effect of transition metal substitution on the catalytic activity of magnetite in heterogeneous Fenton reaction: In interfacial view. Colloids and Surfaces A: Physicochemical and Engineering Aspects, 2013, 435, 28-35.	4.7	54
172	A comparative study about the effects of isomorphous substitution of transition metals (Ti, Cr, Mn,) Tj ETQq0 29-34.	0 0 rgBT /0v 4.8	verlock 10 Tf 70
173	Characterization and catalytic performance of Fe3Ni8/palygorskite for catalytic cracking of benzene. Applied Clay Science, 2013, 74, 135-140.	5.2	33
174	Ecological Risk Assessment of Organochlorine Pesticides in Surface Waters of Lake Taihu, China. Human and Ecological Risk Assessment (HERA), 2013, 19, 840-856.	3.4	13
175	Locking effect: A novel insight in the silylation of montmorillonite surfaces. Materials Chemistry and Physics, 2012, 136, 292-295.	4.0	48
176	Heterogeneous UV/Fenton degradation of TBBPA catalyzed by titanomagnetite: Catalyst characterization, performance and degradation products. Water Research, 2012, 46, 4633-4644.	11.3	164
177	Changes in Structure, Morphology, Porosity, and Surface Activity of Mesoporous Halloysite Nanotubes Under Heating. Clays and Clay Minerals, 2012, 60, 561-573.	1.3	162
178	Distribution characteristics and ecological risk assessment of PAHs in surface waters of China. Science China Earth Sciences, 2012, 55, 914-925.	5.2	29
179	The influence of alkyl chain length on surfactant distribution within organo-montmorillonites and their thermal stability. Journal of Thermal Analysis and Calorimetry, 2012, 109, 301-309.	3.6	33
180	The application of chromium substituted magnetite as heterogeneous Fenton catalyst for the degradation of aqueous cationic and anionic dyes. Chemical Engineering Journal, 2012, 191, 177-184.	12.7	110

#	Article	IF	CITATIONS
181	The contribution of vanadium and titanium on improving methylene blue decolorization through heterogeneous UV-Fenton reaction catalyzed by their co-doped magnetite. Journal of Hazardous Materials, 2012, 199-200, 247-254.	12.4	95
182	Gaseous Elemental Mercury Capture from Flue Gas Using Magnetic Nanosized (Fe <sub>3-<i>x</i></sub> Mn <sub><i>x</i></sub> ) <sub>1-1</sub> O <sub>4</sub> . Environmental Science & Technology, 2011, 45, 1540-1546.	10.0	161
183	Silylation of layered double hydroxides via an induced hydrolysis method. Journal of Materials Chemistry, 2011, 21, 10711.	6.7	37
184	Elemental Mercury Capture from Flue Gas by Magnetic Mn–Fe Spinel: Effect of Chemical Heterogeneity. Industrial & Engineering Chemistry Research, 2011, 50, 9650-9656.	3.7	111
185	A Critical Textural Evolution Study of Zerovalent Iron/Montmorillonite Nanosized Heterostructures Under Various Iron Loadings. Clays and Clay Minerals, 2011, 59, 490-500.	1.3	8
186	Expansion characteristics of organo montmorillonites during the intercalation, aging, drying and rehydration processes: Effect of surfactant/CEC ratio. Colloids and Surfaces A: Physicochemical and Engineering Aspects, 2011, 384, 401-407.	4.7	29
187	Preparation and characterization of zwitterionic surfactant-modified montmorillonites. Journal of Colloid and Interface Science, 2011, 360, 386-392.	9.4	70
188	Silylation of Layered Double Hydroxides via a Calcinationâ^'Rehydration Route. Langmuir, 2010, 26, 2769-2773.	3.5	30
189	Structural and sorptive characteristics of the cetyltrimethylammonium and polyacrylamide modified bentonite. Chemical Engineering Journal, 2010, 160, 220-225.	12.7	28
190	Removal of hexavalent chromium [Cr(VI)] from aqueous solutions by the diatomite-supported/unsupported magnetite nanoparticles. Journal of Hazardous Materials, 2010, 173, 614-621.	12.4	327
191	The decolorization of Acid Orange II in non-homogeneous Fenton reaction catalyzed by natural vanadium–titanium magnetite. Journal of Hazardous Materials, 2010, 181, 112-120.	12.4	109
192	Synthesis, characterization and size control of zerovalent iron nanoparticles anchored on montmorillonite. Science Bulletin, 2010, 55, 1092-1099.	1.7	36
193	Thermal decomposition of silylated layered double hydroxides. Journal of Thermal Analysis and Calorimetry, 2010, 101, 153-159.	3.6	18
194	Infrared investigation of organo-montmorillonites prepared from different surfactants. Spectrochimica Acta - Part A: Molecular and Biomolecular Spectroscopy, 2010, 76, 122-129.	3.9	100
195	Enhancing the sorption capacity of CTMA-bentonite by simultaneous intercalation of cationic polyacrylamide. Journal of Hazardous Materials, 2010, 178, 1078-1084.	12.4	22
196	The remarkable effect of vanadium doping on the adsorption and catalytic activity of magnetite in the decolorization of methylene blue. Applied Catalysis B: Environmental, 2010, 97, 151-159.	20.2	98
197	Organoclays prepared from montmorillonites with different cation exchange capacity and surfactant configuration. Applied Clay Science, 2010, 48, 67-72.	5.2	226
198	Influences of thermal pretreatment temperature and solvent on the organosilane modification of Al13-intercalated/Al-pillared montmorillonite. Applied Clay Science, 2010, 50, 546-553.	5.2	35

#	Article	IF	CITATIONS
199	Sorption of perfluorooctane sulfonate on organo-montmorillonites. Chemosphere, 2010, 78, 688-694.	8.2	119
200	Nanomaterials based upon silylated layered double hydroxides. Applied Surface Science, 2009, 255, 4334-4340.	6.1	73
201	Preparation and characterization of 3-aminopropyltriethoxysilane grafted montmorillonite and acid-activated montmorillonite. Science Bulletin, 2009, 54, 265-271.	9.0	27
202	Montmorillonite-supported magnetite nanoparticles for the removal of hexavalent chromium [Cr(VI)] from aqueous solutions. Journal of Hazardous Materials, 2009, 166, 821-829.	12.4	446
203	Core–shell structured iron nanoparticles well dispersed on montmorillonite. Journal of Magnetism and Magnetic Materials, 2009, 321, 3515-3519.	2.3	51
204	Decolorization of methylene blue by heterogeneous Fenton reaction using Fe3â^'xTixO4 (0≤â‰0.78) at neutral pH values. Applied Catalysis B: Environmental, 2009, 89, 527-535.	20.2	170
205	Degradation of Methylene Blue by Heterogeneous Fenton Reaction Using Titanomagnetite at Neutral pH Values: Process and Affecting Factors. Industrial & Engineering Chemistry Research, 2009, 48, 9915-9921.	3.7	57
206	Effect of surfactant concentration on the stacking modes of organo-silylated layered double hydroxides. Applied Clay Science, 2009, 45, 262-269.	5.2	46
207	In situ synthesis of surfactant/silane-modified hydrotalcites. Journal of Colloid and Interface Science, 2008, 319, 498-504.	9.4	64
208	A combined study by XRD, FTIR, TG and HRTEM on the structure of delaminated Fe-intercalated/pillared clay. Journal of Colloid and Interface Science, 2008, 324, 142-149.	9.4	167
209	Application of near infrared spectroscopy for the determination of adsorbed p-nitrophenol on HDTMA organoclay—implications for the removal of organic pollutants from water. Spectrochimica Acta - Part A: Molecular and Biomolecular Spectroscopy, 2008, 69, 835-841.	3.9	54
210	Quantification of crop residue burning in the field and its influence on ambient air quality in Suqian, China. Atmospheric Environment, 2008, 42, 1961-1969.	4.1	135
211	Synthesis and infrared spectroscopic characterization of selected layered double hydroxides containing divalent Ni and Co. Materials Chemistry and Physics, 2008, 112, 869-875.	4.0	43
212	Changes in the surfaces on DDOAB organoclays adsorbed with paranitrophenol—An XRD, TEM and TG study. Materials Research Bulletin, 2008, 43, 3318-3326.	5.2	6
213	Adsorption ofp-Nitrophenol on Mono-, Di-, and Trialkyl Surfactant-Intercalated Organoclays:  A Comparative Study. Journal of Physical Chemistry C, 2007, 111, 7487-7493.	3.1	27
214	A X-ray photoelectron spectroscopy study of HDTMAB distribution within organoclays. Spectrochimica Acta - Part A: Molecular and Biomolecular Spectroscopy, 2007, 66, 1180-1188.	3.9	55
215	FTIR investigation of CTAB–Al–montmorillonite complexes. Spectrochimica Acta - Part A: Molecular and Biomolecular Spectroscopy, 2007, 67, 1030-1036.	3.9	133
216	Modification of the surfaces of Wyoming montmorillonite by the cationic surfactants alkyl trimethyl, dialkyl dimethyl, and trialkyl methyl ammonium bromides. Journal of Colloid and Interface Science, 2007, 305, 150-158.	9.4	258

#	Article	IF	CITATIONS
217	Changes in the surfaces of adsorbed para-nitrophenol on HDTMA organoclay—The XRD and TG study. Journal of Colloid and Interface Science, 2007, 307, 50-55.	9.4	89
218	TEM, XRD, and thermal stability of adsorbed paranitrophenol on DDOAB organoclay. Journal of Colloid and Interface Science, 2007, 311, 24-37.	9.4	48
219	Thermal stability of octadecyltrimethylammonium bromide modified montmorillonite organoclay. Journal of Colloid and Interface Science, 2007, 311, 347-353.	9.4	105
220	Grafting of montmorillonite with different functional silanes via two different reaction systems. Journal of Colloid and Interface Science, 2007, 313, 268-273.	9.4	106
221	Changes in the surfaces of adsorbed p-nitrophenol on methyltrioctadecylammonium bromide organoclay—An XRD, TG, and infrared spectroscopic study. Journal of Colloid and Interface Science, 2007, 314, 405-414.	9.4	31
222	Microstructure of HDTMA <sup>+</sup> -modified montmorillonite and its influence on sorption characteristics. Clays and Clay Minerals, 2006, 54, 689-696.	1.3	149
223	Changes in the morphology of organoclays with HDTMA+ surfactant loading. Applied Clay Science, 2006, 31, 262-271.	5.2	285
224	Influences of pretreatment temperature on the surface silylation of diatomaceous amorphous silica with trimethylchlorosilane. Journal of Non-Crystalline Solids, 2006, 352, 3762-3771.	3.1	54
225	Synthesis and characterization of delaminated iron-pillared clay with meso–microporous structure. Microporous and Mesoporous Materials, 2006, 88, 8-15.	4.4	104
226	Investigation on the delaminated-pillared structure of TiO2-PILC synthesized by TiCl4 hydrolysis method. Microporous and Mesoporous Materials, 2006, 93, 240-247.	4.4	68
227	Synthesis and characterization of layered double hydroxides with a high aspect ratio. Journal of Solid State Chemistry, 2006, 179, 708-715.	2.9	68
228	Influence of cationic surfactant removal on the thermal stability of organoclays. Journal of Colloid and Interface Science, 2006, 295, 202-208.	9.4	81
229	A novel organoclay with antibacterial activity prepared from montmorillonite and Chlorhexidini Acetas. Journal of Colloid and Interface Science, 2006, 297, 235-243.	9.4	98
230	Arrangement, conformation, and mobility of surfactant molecules intercalated in montmorillonite prepared at different pillaring reagent concentrations as studied by solid-state NMR spectroscopy. Journal of Colloid and Interface Science, 2006, 299, 754-760.	9.4	32
231	Infrared spectroscopy of organoclays synthesized with the surfactant octadecyltrimethylammonium bromide. Spectrochimica Acta - Part A: Molecular and Biomolecular Spectroscopy, 2005, 61, 515-525.	3.9	112
232	Grafting of swelling clay materials with 3-aminopropyltriethoxysilane. Journal of Colloid and Interface Science, 2005, 288, 171-176.	9.4	236
233	The Influence of Random Defect Density on the Thermal Stability of Kaolinites. Journal of the American Ceramic Society, 2005, 88, 1017-1019.	3.8	12
234	Characterization of organic phases in the interlayer of montmorillonite using FTIR and 13C NMR. Journal of Colloid and Interface Science, 2005, 286, 239-244.	9.4	168

#	Article	IF	CITATIONS
235	Modification of Wyoming Montmorillonite Surfaces Using a Cationic Surfactant. Langmuir, 2005, 21, 8675-8680.	3.5	251
236	Molecular Simulation of the Interlayer Structure and the Mobility of Alkyl Chains in HDTMA+/Montmorillonite Hybrids. Journal of Physical Chemistry B, 2005, 109, 13301-13306.	2.6	75
237	Thermal characterization of surfactant-modified montmorillonites. Clays and Clay Minerals, 2005, 53, 287-293.	1.3	187
238	and MAS NMR spectra of mullites from different kaolinites. Spectrochimica Acta - Part A: Molecular and Biomolecular Spectroscopy, 2004, 60, 1061-1064.	3.9	62
239	Raman spectroscopic study of organo-montmorillonites. Journal of Raman Spectroscopy, 2004, 35, 316-323.	2.5	38
240	Structure of organoclays—an X-ray diffraction and thermogravimetric analysis study. Journal of Colloid and Interface Science, 2004, 277, 116-120.	9.4	303
241	Conformation of Surfactant Molecules in the Interlayer of Montmorillonite Studied by <sup>13</sup> C MAS NMR. Clays and Clay Minerals, 2004, 52, 350-356.	1.3	100
242	Arrangement models of alkylammonium cations in the interlayer of HDTMA+ pillared montmorillonites. Science Bulletin, 2003, 48, 368-372.	1.7	67
243	A microstructural study of acid-activated montmorillonite from Choushan, China. Clay Minerals, 2002, 37, 337-344.	0.6	44
244	Experimental study of the selective adsorption of heavy metals onto clay minerals. Diqiu Huaxue, 2000, 19, 105-109.	0.5	30
245	A Review of the Role of Natural Clay Minerals as Effective Adsorbents and an Alternative Source of Minerals. , 0, , .		4